Experimentation and Theoretic Calculation of a BODIPY Sensor Based on Photoinduced Electron Transfer for Ions Detection

Hua Lu,[†] ShuShu Zhang,[‡] HanZhuang Liu,[†] YanWei Wang,[†] Zhen Shen,*[,†] ChunGen Liu,*[,‡] and XiaoZeng You*[,†]

State Key Laboratory of Coordination Chemistry, Nanjing National Laboratory of Microstructures and Institute of Theoretical and Computational Chemistry, Key Laboratory of Mesoscopic Chemistry of the Ministry of Education (MOE), School of Chemistry and Chemical Engineering, Nanjing University, Nanjing 210093, China

Received: July 30, 2009; Revised Manuscript Received: October 22, 2009

A boron-dipyrromethene (BODIPY)-based fluorescence probe with a *N*,*N*′-(pyridine-2, 6-diylbis(methylene))-dianiline substituent (**1**) has been prepared by condensation of 2,6-pyridinedicarboxaldehyde with 8-(4-amino)-4,4-difluoro-1,3,5,7-tetramethyl-4-bora-3a,4a-diaza-*s*-indacene and reduction by $NaBH_4$. The sensing properties of compound **1** toward various metal ions are investigated via fluorometric titration in methanol, which show highly selective fluorescent turn-on response in the presence of Hg^{2+} over the other metal ions, such as Li^+, Na^+, K^+, Ca^{2+}, Mg^{2+}, Pb^{2+}, Fe^{2+}, Co^{2+}, Ni^{2+}, Cu^{2+}, Zn^{2+}, Cd^{2+}, Ag^+, and Mn^{2+}. Computational approach has been carried out to investigate the mechanism why compound **1** provides different fluorescent signal for Hg^{2+} and other ions. Theoretic calculations of the energy levels show that the quenching of the bright green fluorescence of boradiazaindacene fluorophore is due to the reductive photoinduced electron transfer (PET) from the aniline subunit to the excited state of BODIPY fluorophore. In metal complexes, the frontier molecular orbital energy levels changes greatly. Binding Zn^{2+} or Cd^{2+} ion leads to significant decreasing of both the HOMO and LUMO energy levels of the receptor, thus inhibit the reductive PET process, whereas an oxidative PET from the excited state fluorophore to the receptor occurs, vice versa, which also quenches the fluorescence. However, for **1**-Hg^{2+} complex, both the reductive and oxidative PETs are prohibited; therefore, strong fluorescence emission from the fluorophore can be observed experimentally. The agreement of the experimental results and theoretic calculations suggests that our calculation method can be applicable as guidance for the design of new chemosensors for other metal ions.

1. Introduction

The design of chemosensors for monitoring biologically and environmentally important ions in solution, especially heavy and transition-metal (HTM) ions, is currently of great importance.[1] Among HTM ions, Hg^{2+} ions is a highly toxic element and is widely distributed in air, water, and soil because mercury and mercuric salts are used in many industrial processes and products such as chemical manufacturing or as mining byproducts.[2] Therefore, it is very important to develop sensitive and selective sensors for Hg^{2+}. Currently, remarkable progress in the design, synthesis, and characterization of Hg^{2+}-responsive sensors has been made over the past several years.[3] However, mechanistic studies and theoretic calculations aimed at providing detailed explanations of how individual sensor provide different optical feedback for Hg^{2+} and other ions are often lacking, and such research will guide the design of next-generation sensors with improved properties.[3a]

Recent efforts in our laboratory have focused on developing BODIPY fluorescence sensors based on photoinduced electron transfer (PET) as a transduction mechanism.[4] BODIPY sensors combine the advantages of high molar extinction coefficients (usually $\varepsilon > 80\,000\ M^{-1}\ cm^{-1}$) and high fluorescence quantum yields (commonly $\Phi_f > 0.50$) and can be excited at relatively long wavelengths (ca. 500 nm).[4b,5] In addition, the BODIPY core has a relatively moderate redox potential, which is a prerequisite when aiming at the construction of fluorescent switches based on electron transfer processes.[4a] For PET sensors, the receptor and fluorophore are usually separated by a (short) alkyl spacer, electronically disconnecting the π-electron systems of receptor and fluorophore. In the unbound state, after excitation, a fast electron transfer from the receptor to the fluorophore quenches the fluorescence of the system. When the receptor is bound, the receptor redox potential is perturbed and slows down the PET process, reviving fluorescence emission; this logic indication can also be reversed.[6] In this work, we evaluate the computational approach in PET sensor and explain why compound **1** provides a different fluorescent signal for Hg^{2+} and other ions.

2. Results and Discussion

2.1. Syntheses. The procedures for the synthesis of BODIPY derivatives **1**−**3** are outlined in Scheme 1. Compound **3**, 8-(4-nitro)-4,4-difluoro-1,3,5,7-tetramethyl-4-bora-3a,4a-diaza-*s*-indacene, was prepared through TFA-catalyzed condensation of 2,4-dimethylpyrrole with 4-nitrobenzaldehyde in a one-pot reaction.[7] The nitro group was subsequently reduced to the amino group using Fe-HCl (yield 85%), which is condensed with 2,6-pyridinedicarboxaldehyde and reduced by $NaBH_4$ to afford the ideal compound **1** (yield 11%).

2.2. Spectroscopic and Detective Properties of 1. The absorption and fluorescence spectra of **1** (Figure 1) show the

* Corresponding authors. E-mail: cgliu@nju.edu.cn (C.L.); zshen@nju.edu.cn (Z.S.).

[†] State Key Laboratory of Coordination Chemistry, Nanjing National Laboratory of Microstructures.

[‡] Institute of Theoretical and Computational Chemistry, Key Laboratory of Mesoscopic Chemistry of the Ministry of Education (MOE), School of Chemistry and Chemical Engineering.

10.1021/jp907331q
Published on Web 12/01/2009

SCHEME 1: Synthetic Procedure for BODIPY 1−3

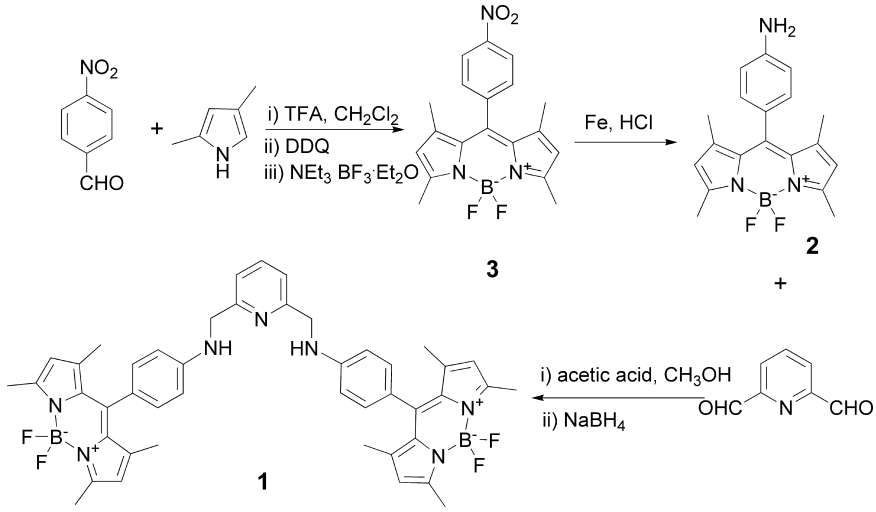

characteristic spectroscopic properties of the BODIPY chromophore with slight stoke shifts. In methanol, a strong S_0-S_1 transition with a maximum at 497 nm ($\varepsilon = 149\,000\ M^{-1}\ cm^{-1}$) and a shoulder at shorter wavelength side is observed.[8] The fluorescence spectrum of **1** displays an emission band at 513 nm with low quantum yield ($\Phi_f = 0.003$) upon excitation at 483 nm due to the PET process from the aniline moiety to the BODIPY fluorophore.[9]

We evaluate the selective properties of **1** toward various metal ions (Figure 2). Upon the addition of 20 equiv Hg^{2+}, the intensity of the emission band at 513 nm increases dramatically, and 32-fold ($\Phi/\Phi_0 = 43$) enhancement is estimated. However, the fluorescence intensity of **1** is almost not influenced by the addition of other metal ions (Li^+, Na^+, K^+, Ca^{2+}, Mg^{2+}, Pb^{2+}, Fe^{2+}, Co^{2+}, Ni^{2+}, Cu^{2+}, Zn^{2+}, Cd^{2+}, Ag^+, and Mn^{2+}, respectively). A very small enhancement by the addition of Al^{3+} ($\Phi/\Phi_0 = 4.2$) is observed. To evaluate the further utility of **1** as an ion-selective fluorescent sensor for Hg^{2+}, the ion interference experiment is carried out (Figure 2, right). The fluorescence intensity is almost identical to that obtained in the absence of interfering metal ions, except that Fe^{2+} has a little influence, but there is still 18-fold enhancement at 513 nm in the presence of 20 equiv Hg^{2+}; these results suggest that **1** could be considered as an effective fluorescent turn-on sensor for Hg^{2+}.

2.3. Theoretic Calculation. Usually, quenching of the original fluorescent emission will take place when the PET process is followed by a nonluminescent adiabatic process returning to the ground state. Besides the famous Marcus theory,[10] which may lead to quantitative description of the kinetics of electron transfer if the coupling between the initial and final states is well accounted, the PET process may also be rationalized pictorially in terms of simple molecular orbital theory, which was first developed by Weller[11] and has become a prevalent tool to discuss the fluorescence on−off problem.[12] According to Weller's approach, after photoinduced electronic excitation from occupied orbitals to unoccupied orbitals, the corresponding orbitals are left singly occupied. Electron transfer process can then be initiated in two situations, where the fluorophore serves either as the electron acceptor or as the electron donor. When the fluorophore serves as the electron acceptor, the HOMO of the fluorophore should be lower than that of the receptor so that an electron on the receptor is capable of transferring to the fuorophore and filling in the singly occupied HOMO. Contrarily, when the fluorophore serves as the electron donor, the LUMO orbital of the fluorophore should be higher than the LUMO of the receptor, which permits the excited electron on the fluorophore to transfer to the unoccupied LUMO of the receptor. Accordingly, the above two PET processes are addressed as reductive-PET and oxidative-PET, respectively.[5c] It is the alternative roles of donor and acceptor for the excited fluorophore that makes PET very complicated.[13]

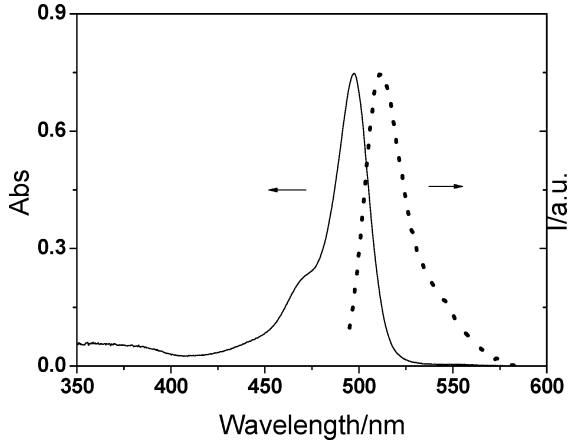

Figure 1. Absorption (solid line) and fluorescence (dotted line) spectra of **1** in methanol.

In many cases, the success of the above oversimplified theoretical approach is owing to the fact that for most chromophores the HOMO−LUMO excitation predominantly contributes to the corresponding excited state, which guarantees the effectiveness of single electron theories. However, the BODIPY fluorophore under investigation is slightly different. It has been commonly accepted that the fluorescence emission of BODIPY is related to the strongest absorption due to S_0 to S_1 excitation. TD-DFT calculation indicates that besides HOMO to LUMO excitation (0.55 participation in excited-state wave function) HOMO-1 to LUMO also has considerable contribution to state S_1 (0.23 participation in excited-state wave function). In this case, our calculation will show that such as in compound **1** the process of electron transfer to BODIPY will be initiated if only the HOMO of the donor is located above the HOMO-1 orbital of BODIPY, as illustrated in Figure 3.

Many researchers tended to evaluate the energy level of the corresponding MOs by computing on the separated electron donor and acceptor, respectively.[12a,14] Because the interaction

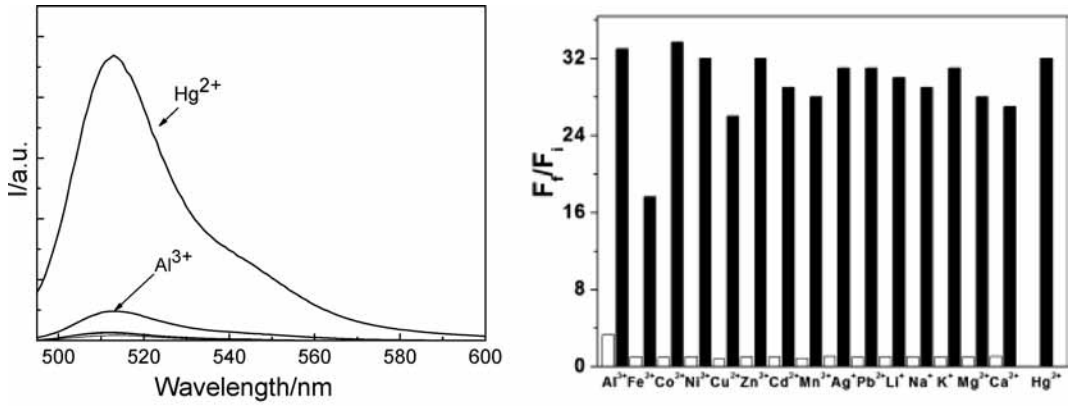

Figure 2. (Left): Fluorescence responses of **1** (5 μM) in the presence of 20 equiv of various cations (Li^+, Mg^{2+}, Na^+, Ca^{2+}, Zn^{2+}, Cu^{2+}, Cd^{2+}, Co^{2+}, K^+, Mn^{2+}, Ni^{2+}, Ag^+, Al^{3+}, Fe^{2+}, Pb^{2+}, and Hg^{2+}) in CH_3OH. (Right): Bars represent the final integrated fluorescence response (F_f) over the initial integrated emission (F_i). White bars represent the addition of 20 equiv different metal ions. Black bars represent the subsequent addition of 20 equiv Hg^{2+} to the solution, $\lambda_{ex} = 483$ nm.

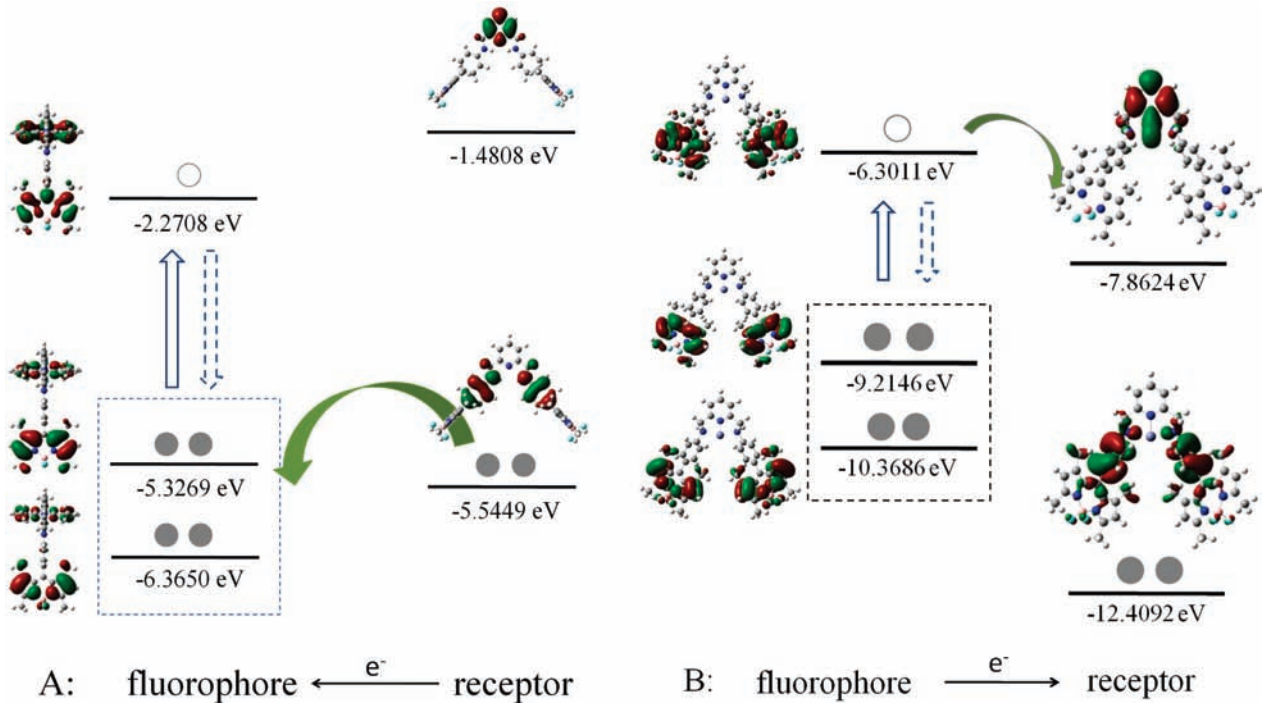

Figure 3. Frontier orbital energy diagrams and electron-transfer paths in **1** (diagram A) and after attachment of Zn^{2+} ion (diagram B).

between the donor and the acceptor is completely neglected, the calculated energy levels as well as molecular orbital diagrams may not precisely represent the real status of the electrons on these orbitals. Furthermore, the energy levels may seriously rely on the partition scheme, which often makes the conclusion quite artificial. In our study, calculations will always be performed on the total system, and we will distinguish the donor orbitals and acceptor orbitals by simply inspecting the orbital distribution diagram. Figure 3 shows the possible pathways of fluorescence emission and electron transfer processes. To obtain these orbital energies, we need to optimize the ground-state structure. Then, we look into the electron distribution and pick out the orbitals mainly localized on fluorophor part to form the left column; similarly, the right column comes from orbitals mainly distributed on the receptor part. The main advantage of this so-called "one-off calculation" is that it overcomes the artificial cut of a whole molecule and reserves the electron correlation between the donor and acceptor parts. Actually, a similar scheme has been adopted by Salman et al.[12d]

As has been previously discussed, the electron transfer from aniline group to BODIPY fluorophore to reach the S_1 state of compound **1** is possible due to the fact that the HOMO of the substituent is located above the HOMO-1 of the BODIPY. Electron transfer takes place during the electrons reorganization to its lowest vibrational state on the S_1 energy surface, which prohibits the electron on the LUMO of BODIPY from going back directly, which could explain the low fluorescence quantum yield of compound **1**. However, when combined with metal ions, the energy levels of the molecular orbitals may change greatly, which might lead to significant changes in energy sequences of these frontier orbitals.

Let us first look at the mercury ion. Experimental observation showed that after being combined with this ion, compound **1** presented a dramatic increase in the intensity of the emission band, which implied that electron transfer process was greatly suppressed in the complex. Geometry optimizations indicate that a stable complex was formed, with significant changes of the conformation of compound **1**, as shown in Figure 4. Rotation of the two aniline groups has been observed, which turns the

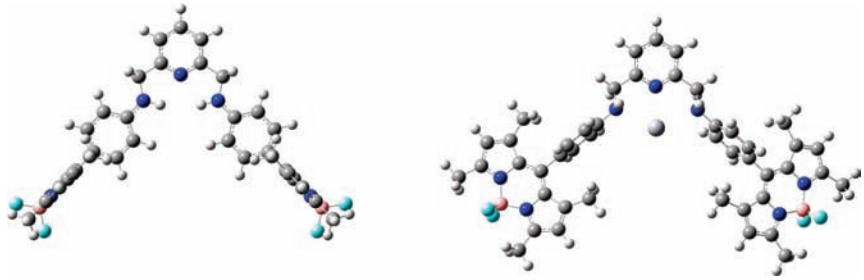

Figure 4. Geometries of **1** and its Hg^{2+} complex calculated with DFT method.

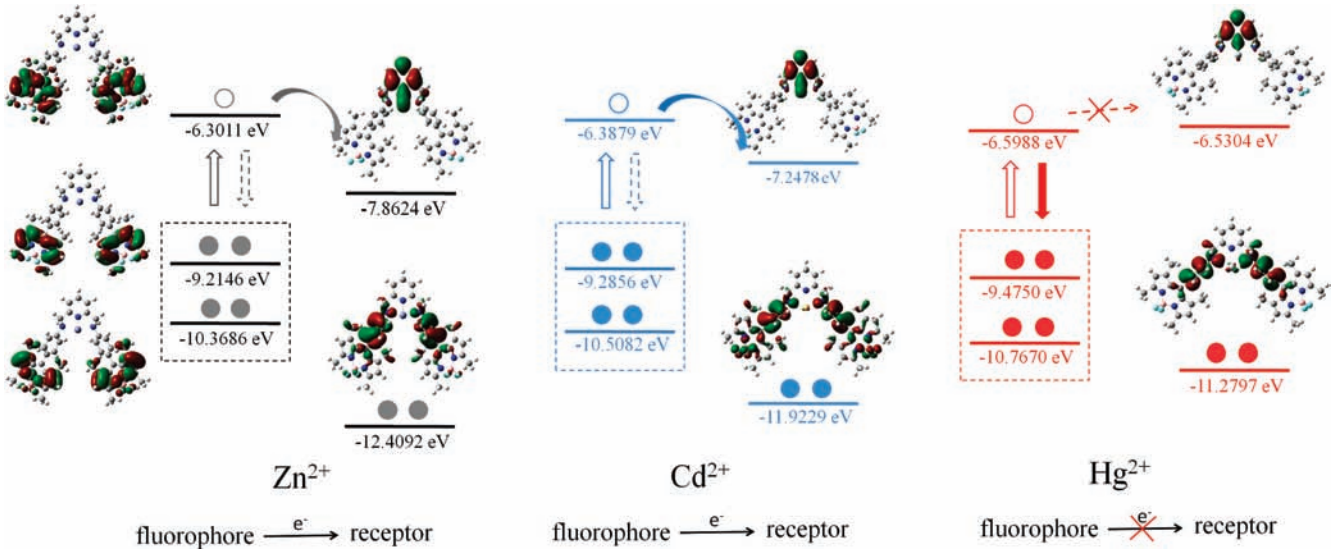

Figure 5. Frontier orbital energy diagrams and electron-transfer paths in metal-attached molecules. The attachment of Zn^{2+} (left column) and Cd^{2+} (middle column) ions provides an efficient electron transfer path, whereas the attachment of Hg^{2+} ion does not.

lone-pair electrons on the nitrogen atoms toward bounded Hg^{2+}. Other metal ions induced similar structure change upon binding with **1**.

It is not surprising that all frontier molecular orbital energy levels in divalent metal−BODIPY complexes are lower than the corresponding ones in compound **1**. Furthermore, the orbitals mainly located close to the coordination center dropped down much further than those localized on the BODIPY segment, which is far from the coordination center. Similar cases are witnessed for metal ions Zn^{2+} and Cd^{2+}, which are illustrated in Figure 5. The way to obtain these relative frontier orbitals has been described before. As we can see, the orbitals distributed on the fluorophore (collected in the left-hand side in Figure 5) almost reserved their nature, as illustrated in Figure 3, whereas the receptor's orbitals (collected in the right-hand side in Figure 5) were affected by the metal ions participation. Consequently, the energy sequence changed significantly. The HOMO orbital of the original substituent in compound **1** is decreased to far below the HOMO-1 orbital of BODIPY, and the reductive-PET process is prohibited. The oxidative-PET might be favored if the LUMO orbital mainly located on the substituent is decreased to below the LUMO of the BODIPY segment. Our calculations indicate that for Zn^{2+} and Cd^{2+} the oxidative-PET is very probable to happen because of the ca. 1 eV energy gap of the two LUMOs. Very interestingly, as could be seen from Figure 5, Hg^{2+} shows a little weaker metal ion effect than Zn^{2+} and Cd^{2+}, and the LUMO orbital of the receptor is still higher than the LUMO of the fluorophore, and the oxidative-PET process cannot be initiated. That explains the fluorescence enhancement phenomena after the addition of the Hg^{2+} ion. The weak emission observed in the presence of Al^{3+} ion shown in Supporting Information Figure S2 might be due to the small energy gap, ca. 0.2 eV, between the LUMOs of the fluorophore and receptor according to our calculation (Supporting Information, Figure S2).

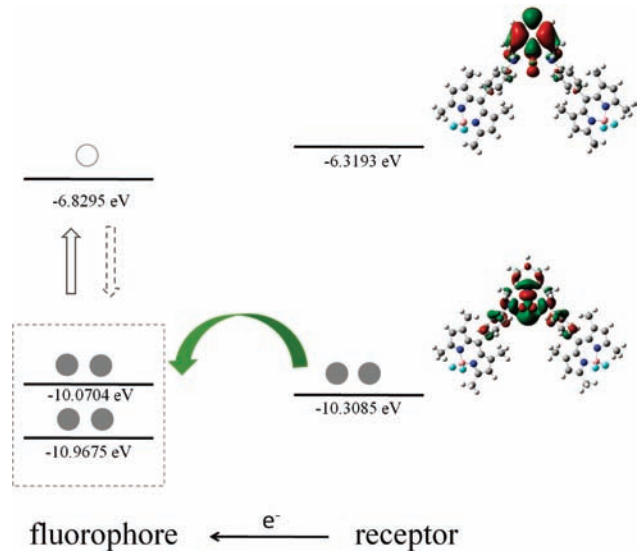

Figure 6. Frontier orbital energy diagram and electron-transfer path in compound **1** after binding Cu^{2+} ion.

The mechanism of the quenching of fluorescence by Cu^{2+} might be very different from that of Zn^{2+} and Cd^{2+}. As shown in Figure 6, the open-shell electronic structure Cu^{2+} ion will significantly influence the HOMO of the substituent. Unlike Zn^{2+}, Cd^{2+}, and Hg^{2+}, the 3d orbitals of Cu^{2+} greatly contributed

to the HOMO orbital and raised this orbital up to a much higher level that is between the HOMO and HOMO-1 of the BODIPY segment. Therefore, the fluorescence may be quenched by a reductive-PET.

3. Conclusions

We have developed a highly selective sensor based on BODIPY for Hg^{2+} and have shown the potential of using theoretic calculations for providing detailed explanations of how compound **1** provides different optical feedback for Hg^{2+} and other ions. In the design of the PET sensor, many factors affect the fluorescence intensity such as electron transfer rate and fluorescence lifetime; however, the more simplistic approach of comparing relative energy levels is useful and effective in the design of PET sensors as guidance. For BODIPY, it is noticed that the HOMO-1 energy level must be considered in the explanation of PET process.

4. Experimental Section

4.1. Materials and Instrumentations. All reagents were obtained from commercial suppliers and used without further purification unless otherwise indicated. All air and moisture-sensitive reactions were carried out under nitrogen atmosphere in oven-dried glassware. Dichloromethane was distilled over calcium hydride. Triethylamine was obtained by simple distillation. NMR spectra were recorded on a Bruker DRX500 spectrometer and referenced to the residual proton signals of the solvent. Mass spectra were measured with a Bruker Daltonics Autoflex^{II} TM MALDI TOF spectrometer. Luminescence spectra were measured on an Aminco Bowman 2 luminescence spectrophotometer. Absorption spectra were measured with a Shimadzu UV3100 apparatus. The fluorescence quantum yield was calculated using Rhodamine 6G ($\Phi_f = 0.88$ in EtOH) as a reference.[15]

4.2. Synthesis of 8-(4-Nitro)-4,4-difluoro-1,3,5,7-tetramethyl-4-bora-3a,4a-diaza-*s*-indacene (3). 2,4-Dimethylpyrrole (380 mg, 4 mmol) and 4-nitrobenzaldehyde (302 mg, 2 mmol) were dissolved in dry CH_2Cl_2 (100 mL) under nitrogen. One drop of trifluoroacetic acid (TFA) was added, and the solution was stirred for 4 h at ambient temperature in the dark. 2,3-Dichloro-5,6-dicyanoquinone (DDQ, 442 mg, 2 mmol) was added, and the mixture was stirred for an additional 20 min. The reaction mixture was then treated with triethylamine (3 mL) for 5 min. Boron trifluoride etherate (3.2 mL) was added and stirred for another 40 min, and the dark-brown solution was washed with water (2 × 20 mL) and brine (30 mL), dried over anhydrous magnesium sulfate, and concentrated at reduced pressure. The crude product was purified by silica-gel flash column chromatography (elution with 10% EtOAc/petroleum ether) and recrystallization from $CHCl_3$/hexane to yield **2** as red crystals (221 mg, yield 30%). ^{1}H NMR (500 MHz, $CDCl_3$, δ): 8.4 (d, $J = 3$ Hz, 2 H), 7.55 (d, $J = 3$ Hz, 2H), 6.03 (s, 2H), 2.58 (s, 6H), 1.37 (s, 6 H).

4.3. Synthesis of 8-(4-Amino)-4,4-difluoro-1,3,5,7-tetramethyl-4-bora-3a,4a-diaza-*s*-indacene (2). Compound **3** (120 mg, 0.325 mmol) was dissolved in 5 mL of methanol. H_2O (2 mL) and Fe powder (300 mg, 5.4 mmol) were added, and the mixture was heated to reflux. Then, the solution of hydrochloric acid in methanol (2 mL, 0.5 mol/L) was added dropwise. The solution was stirred at reflux for 2 h until TLC monitoring indicated complete consumption of the starting material. The reaction mixture was cooled to room temperature, filtrated, and concentrated at reduced pressure. The crude product was purified by silica-gel flash column chromatography (elution with 20% EtOAc/petroleum ether). Recrystallization from $CHCl_3$/hexane yielded crystals (89 mg, yield 85%). ^{1}H NMR (500 MHz, $CDCl_3$, δ): 7.06 (d, $J = 8$ Hz, 2 H), 6.86 (d, $J = 8$ Hz, 2H), 5.99 (s, 2H), 2.57 (s, 6H), 1.51 (s, 6 H). MS (MALDI-TOF): *m*/z 339.19 $[M]^+$, 339.188 $[M\text{-}F]^+$ 320.103.

4.4. Synthesis of Compound 1. Compound **2** (89 mg, 0.26 mmol), 2,6-pyridinedicarboxaldehyde (17 mg, 0.13 mmol), and a catalytic amount of acetic acid in MeOH (10 mL) were refluxed for 24 h. After cooling to the room temperature, $NaBH_4$ (23 mg, 0.6 mmol) was slowly added with stirring, and the reaction mixture was refluxed for a further period of 12 h and concentrated at reduced pressure. The crude product was purified by silica-gel flash column chromatography (elution with 40% EtOAc/petroleum ether). Recrystallization from CH_3OH/hexane yielded red crystals (11 mg, yield 10.9%). Mp > 200 °C. λ_{max} (CH_3OH)/nm: 497 nm ($\varepsilon = 149\,000\ M^{-1}cm^{-1}$). ^{1}H NMR (400 MHz, $CDCl_3$, δ): 7.72 (m, 1 H), 7.28 (m, 2 H), 7.02 (d, $J = 8.2$ Hz, 4H), 6.78 (d, $J = 8.2$ Hz, 4H), 5.96 (s, 4H), 4.58 (s, 4H), 2.54 (s, 12H), 1.48 (s, 12H). MS (MALDI-TOF): *m/z* 762.366 $[M\text{-}F]^+$, 734.3 $[M\text{-}2F]^+$. HRMS-EI: calcd for $C_{45}H_{45}B_2F_4N_7Na$ $[M+Na]^+$, 804.3756; found $[M+Na]^+$, 804.3751

4.5. Procedures for Metal Ion Sensing. Stock solutions of the metal ions (10 mM) were prepared in deionized water. A stock solution of **1** (0.5 mM) was prepared in CH_3OH and then diluted to 5 μM with CH_3OH. In titration experiments, each time, a 2 mL solution of **1** (5 μM) was filled in a quartz optical cell of 1 cm optical path length, and the Hg^{2+} stock solution was added to the quartz optical cell gradually by using a micropipet. Spectral data were recorded immediately after the addition. In selectivity experiments, the test samples were prepared by placing appropriate amounts of metal ion solution into 2 mL of solution of **1** (5 μM). For fluorescence measurements, excitation was provided at 483 nm, and emission was collected from 495 to 600 nm.

4.6. Computational Details. The ground-state structures of BODIPY-based compound **1** and its several metal complexes were computed using the density functional theory (DFT) method with the hybrid-generalized gradient approximation (H-GGA) functional B3LYP. Double valence 3-21g basis set was assigned to nonmetal elements (C, H, N, B, and F), which guarantees a reasonable balance of the computational cost and the reliability of the results. For the metal elements under investigation, the effective core potential LanL2DZ basis sets were employed to incorporate the relativistic corrections. The absorption properties were predicted by time-dependent (TD-DFT) method. All of the calculations were performed with the Gaussian03 program package.[16]

Acknowledgment. We are thankful for the financial support from the National Basic Research Program of China (nos. 2006CB806104 and 2007CB925103 to Z.S. and X.Z.Y.), NSFC (nos. 20971066 and 20875043 to Z.S. and 20873058 to C.-G.L.).

Supporting Information Available: Fluorescence response of compound **1** in the presence of increasing amount of Hg^{2+}, frontier orbital energy diagram and electron-transfer path in compound **1** after binding with Al^{3+}, Ag^+, and Ni^{2+}, and ^{1}HNMR spectra of compound **1**. This material is available free of charge via the Internet at http://pubs.acs.org

References and Notes

(1) (a) Amendola, V.; Fabbrizzi, L.; Licchelli, M.; Mangano, C.; Pallavicini, P.; Parodi, L.; Poggi, A. *Coord. Chem. Rev.* **1999**, *190−192*, 649–669. (b) Prodi, L.; Bolletta, F.; Montalti, M.; Zaccheroni, N. *Coord. Chem. Rev.* **2000**, *205*, 59–83. (c) Rurack, K. *Spectrochimica Acta., Part*

A **2001**, *57*, 2161–2195. (d) Que, E. L.; Domaille, D. W.; Chang, C. J. *Chem. Rev.* **2008**, *108*, 1517–1549. (e) Kim, H. N.; Lee, M. H.; Kim, H. J.; Kim, J. S.; Yoon, J. *Chem. Soc. Rev.* **2008**, *37*, 1465–1472.

(2) (a) Descalzo, A. B.; Martínez-Máñez, R.; Radeglia, R.; Rurack, K.; Soto, J. *J. Am. Chem. Soc.* **2003**, *125*, 3418–3419. (b) Boening, D. W. *Chemosphere* **2000**, *40*, 1335–1351.

(3) For a recent review, see: (a) Nolan, E. M.; Lippard, S. J. *Chem. Rev.* **2008**, *108*, 3443–3480. For selected examples, see: (b) Choi, S. H.; Pang, K.; Kim, K.; Churchill, D. G. *Inorg. Chem.* **2007**, *46*, 10564–10577. (c) Yuan, M. J.; Li, Y. L.; Li, J. B.; Li, C. H.; Liu, X. F.; Lv, J.; Xu, J. L.; Liu, H. B; Wang, S.; Zhu, D. B. *Org. Lett.* **2007**, *9*, 2313–2316. (d) Yuan, M.; Zhou, W.; Liu, X.; Zhu, M.; Li, J.; Yin, X.; Zheng, H.; Zuo, Z.; Ouyang, C.; Liu, H.; Li, Y.; Zhu, D. *J. Org. Chem.* **2008**, *73*, 5008–5014. (e) Zhang, X.; Xiao, Y.; Qian, X. *Angew. Chem., Int. Ed.* **2008**, *47*, 8025–8029. (f) Chen, X.; Nam, S. W.; Jou, M. J.; Kim, Y.; Kim, S. J.; Park, S.; Yoon, J. *Org. Lett.* **2008**, *10*, 5235–5238. (g) Suresh, M; Shrivastav, A; Mishra, S; Suresh, E; Das, A. *Org. Lett.* **2008**, *10*, 3013–3016. (h) Domaille, D. W.; Que, E. L; Chang, C. J. *Nat. Chem. Biol.* **2008**, *4*, 168–175. (i) Lu, H.; Xiong, L. Q.; Liu, H. Z.; Yu, M. X.; Shen, Z.; Li, F. Y.; You, X. Z. *Org. Biomol. Chem.* **2009**, *7*, 2554–2558.

(4) (a) Shen, Z.; Roehr, H.; Rurack, K.; Uno, H.; Spieles, M.; Schulz, B.; Reck, G.; Ono, N. *Chem.—Eur. J.* **2004**, *10*, 4853–4871. (b) Yu, Y. H.; Descalzo, A. B.; Shen, Z.; Röhr, H.; Liu, Q.; Wang, Y. W.; Spieles, M.; Li, Y. Z.; Rurack, K.; You, X. Z. *Chem. Asian J.* **2006**, *1*, 176–187. (c) Descalzo, A. B.; Xu, H. J.; Xue, Z. L.; Hoffmann, K.; Shen, Z.; Weller, M. G.; You, X. Z.; Rurack, K. *Org. Lett.* **2008**, *10*, 1581–1584. (d) Yu, Y. H.; Shen, Z.; Xu, H. Y.; Wang, Y. W.; Okujima, T.; Ono, N.; Li, Y. Z.; You, X. Z. *J. Mol. Struct.* **2007**, *827*, 130–136. (e) Wang, Y. W.; Li, M.; Shen, Z.; You, X. Z. *Chin. J. Inorg. Chem.* **2008**, *24*, 1247–1252. (f) Xu, H. Y.; Shen, Z.; Okujima, T.; Ono, N. *Chin. J. Inorg. Chem.* **2006**, *22*, 801–807.

(5) (a) Baruah, M.; Qin, W.; Flors, C.; Hofkens, J.; Vallée, R. A. L.; Beljonne, D.; Van der Auweraer, M.; De Borggraeve, W. M.; Boens, N. *J. Phys. Chem. A* **2006**, *110*, 5998–6009. (b) Ulrich, G.; Ziessel, R.; Harriman, A. *Angew. Chem., Int. Ed.* **2008**, *47*, 1184–1201. (c) Loudet, A.; Burgess, K. *Chem. Rev.* **2007**, *107*, 4891–4932. (d) Qin, W.; Baruah, M.; Sliwa, M.; Van der Auweraer, M.; De Borggraeve, W. M.; Beljonne, D.; Van Averbeke, B. V.; Boens, N. *J. Phys. Chem. A* **2008**, *112*, 6104–6114.

(6) Rurack, K.; Resch-Genger, U. *Chem. Soc. Rev.* **2002**, *31*, 116–127.

(7) Rurack, K.; Kollmannsberger, M.; Daub, J. *Angew. Chem., Int. Ed.* **2001**, *40*, 385–387.

(8) (a) Qin, W.; Baruah, M.; Van der Auweraer, M.; Frans, C.; De Schryver, F. C.; Boens, N. *J. Phys. Chem, A* **2005**, *109*, 7371–7384. (b) Costela, A.; Garcïa-Moreno, I.; Gomez, C.; Sastre, R.; Amat-Guerri, F.; Liras, M.; López Arbeloa, F.; Bañuelos Prieto, J.; Lípez Arbeloa, I. *J. Phys. Chem. A* **2002**, *106*, 7736–7742. (c) Lípez Arbeloa, F.; Bañuelos Prieto, J.; Martíanez, V.; Arbeloa López, T.; Lípez Arbeloa, I. *ChemPhysChem* **2004**, *5*, 1762–1771.

(9) Kollmannsberger, M.; Rurack, K.; Resch-Genger, U.; Daub, J. *J. Phys. Chem. A* **1998**, *102*, 10211–10220.

(10) Marcus, R. A. *Angew. Chem., Int. Ed. Engl.* **1993**, *32*, 1111–1121.

(11) Weller, A. *Pure Appl. Chem.* **1968**, *16*, 115.

(12) (a) Bañuelos, J.; Arbeloa, F. L.; Arbeloa, T.; Salleres, S.; Amat-Guerri, F.; Liras, M.; Arbeloa, I. L. *J. Phys. Chem. A* **2008**, *112*, 10816–10822. (b) Fan, L. J.; Zhang, Y.; Murphy, C. B.; Angell, S. E.; Parker, M. F. L.; Flynn, B. R.; Jones, W. E. *Coord. Chem. Rev.* **2009**, *253*, 410–422. (c) De Silva, A. P.; Gunaratne, H. Q. N.; Gunnlaugsson, T.; Huxley, A. J. M.; McCoy, C. P.; Rademacher, J. T.; Rice, T. E. *Chem. Rev.* **1997**, *97*, 1515–1566. (d) Salman, H.; Tal, S.; Chuvilov, Y.; Solovey, O.; Abraham, Y.; Kapon, M.; Suwinska, K.; Eichen, Y. *Inorg. Chem.* **2006**, *45*, 5315–5320.

(13) Lakowicz, J. R. In *Principles of Fluorescence Spectroscopy*, 3rd ed.; Springer: New York, 2006; pp 335−336.

(14) (a) McCarroll, M. E.; Shi, Y.; Harris, S.; Puli, S.; Kimaru, I.; Xu, R. S.; Wang, L. C.; Dyer, D. *J. Phys. Chem. B* **2006**, *110*, 22991–22994. (b) Kennedy, D. P.; Kormos, C. M.; Burdette, S. C. *J. Am. Chem. Soc.* **2009**, *131*, 8578.

(15) Olmsted, J. *J. Phys. Chem.* **1979**, *83*, 2581–2584.

(16) Frisch, M. J.; Trucks, G. W.; Schlegel, H. B.; Scuseria, G. E.; Robb, M. A.; Cheeseman, J. R.; Montgomery, J. A., Jr.; Vreven, T.; Kudin, K. N.; Burant, J. C.; Millam, J. M.; Iyengar, S. S.; Tomasi, J.; Barone, V.; Mennucci, B.; Cossi, M.; Scalmani, G.; Rega, N.; Petersson, G. A.; Nakatsuji, H.; Hada, M.; Ehara, M.; Toyota, K.; Fukuda, R.; Hasegawa, J.; Ishida, M.; Nakajima, T.; Honda, Y.; Kitao, O.; Nakai, H.; Klene, M.; Li, X.; Knox, J. E.; Hratchian, H. P.; Cross, J. B.; Bakken, V.; Adamo, C.; Jaramillo, J.; Gomperts, R.; Stratmann, R. E.; Yazyev, O.; Austin, A. J.; Cammi, R.; Pomelli, C.; Ochterski, J. W.; Ayala, P. Y.; Morokuma, K.; Voth, G. A.; Salvador, P.; Dannenberg, J. J.; Zakrzewski, V. G.; Dapprich, S.; Daniels, A. D.; Strain, M. C.; Farkas, O.; Malick, D. K.; Rabuck, A. D.; Raghavachari, K.; Foresman, J. B.; Ortiz, J. V.; Cui, Q.; Baboul. G.; Clifford, S.; Cioslowski, J.; Stefanov, B. B.; Liu, G.; Liashenko, A.; Piskorz, P.; Komaromi, I.; Martin, R. L.; Fox, D. J.; Keith, T.; Al-Laham, M. A.; Peng, C. Y.; Nanayakkara, A.; Challacombe, M.; Gill, P. M. W.; Johnson, B.; Chen, W.; Wong, M. W.; Gonzalez, C.; Pople, J. A. *Gaussian 03*, revision D.01; Gaussian, Inc.: Wallingford CT, 2004.

JP907331Q